

A unified framework for Bell inequalities from continuous-variable contextuality

C. E. Lopetegui-González,^{1,*} G. Massé,² E. Oudot,² U. I. Meyer,² F. Centrone,^{3,4} F. Grosshans,² P. E. Emeriau,⁵ U. Chabaud,⁶ and M. Walschaers^{1,†}

¹*Laboratoire Kastler Brossel, Sorbonne Université, CNRS, ENS-Université PSL, Collège de France, 4 place Jussieu, Paris F-75252, France*

²*Sorbonne Université, CNRS, LIP6*

³*ICFO-Institut de Ciències Fotoniques, The Barcelona Institute of Science and Technology*

⁴*Universidad de Buenos Aires, Instituto de Física de Buenos Aires (IFIBA)*

⁵*Quandela, 7 rue Léonard de Vinci, 91300 Massy, France*

⁶*DIENS, École Normale Supérieure, PSL University, CNRS, INRIA, 45 rue d'Ulm, Paris, 75005, France*

(Dated: January 13, 2026)

Although the original EPR paradox was formulated in terms of position and momentum, most studies of these phenomena have focused on measurement scenarios with only a discrete number of possible measurement outcomes. Here, we present a framework for studying non-locality that is agnostic to the dimension of the physical systems involved, allowing us to probe purely continuous-variable, discrete-variable, or hybrid non-locality. Our approach allows us to find the optimal Bell inequality for any given measurement scenario and quantifies the amount of non-locality that is present in measurement statistics. This formalism unifies the existing literature on continuous-variable non-locality and allows us to identify new states in which Bell non-locality can be probed through homodyne detection. Notably, we find the first example of continuous-variable non-locality that cannot be mapped to a CHSH Bell inequality. Moreover, we provide several examples of simple hybrid DV-CV entangled states that could lead to near-term violation of Bell inequalities.

I. INTRODUCTION

The inconsistency of the predictions of quantum theory with local realism was first pointed out by Einstein, Podolsky and Rosen in [1]. For a long time the subject of philosophical debates, it was the work of Bell [2] that transformed this inconsistency into a quantifiable, experimentally testable claim, namely the violation of a Bell inequality. Several experiments have been performed since the advent of Bell's inequalities to probe the non-local features of quantum mechanics, with an increasing level of refinement [3–8].

Beyond its fundamental interest, non-locality has emerged as a key resource for applications such as device-independent quantum information processing [9], where the violation of a Bell inequality serves as a security guarantee. To deploy such protocols in practice, optical implementations with room-temperature detectors are desirable. Homodyne detection of the quadratures of an electromagnetic field [10], offers such detection capabilities for continuous-variable (CV) quantum information processing on traveling modes of light [11]. However, violating Bell inequalities in such systems remains a big challenge, despite extensive theoretical efforts [12–20].

Most of the proposals for performing Bell tests on CV systems rely on imposing a predefined binning strategy, that maps the continuum of possible outcomes to either 1 or -1 , to then apply the Clauser–Horne–Shimony–Holt (CHSH) inequality [21]. In [18], using similar binning

strategies, the Mermin–Klyshko inequality [22, 23] was used to probe non-locality for more than two modes, which should allow to obtain larger normalized Bell inequality violations than what is possible with CHSH [24]. Recent efforts have been devoted to automatizing the binning procedure [20], leading to considerable improvements in the expected violation of the local bounds. Nevertheless, the procedure is constrained to states with a limited number of photons. A genuinely CV Bell inequality has only been proposed in [17], which does not rely on any discretization of the continuum of measurement outcomes, but rather on a non-linear combination of their moments. The down-side of this approach is that at least ten modes are required to obtain a violation of the local bound. Therefore, its relevance for an experimental implementation remains limited, despite the theoretical appeal of this inequality.

The point that all the above approaches have in common is that they start from a Bell inequality without any guarantee that it will be practical for the measurement scenario at hand. Our general framework takes a radically different approach in that it starts from experimental measurement data and finds the optimal Bell inequality associated with them. For this, we also discretize the outcomes, but not as a predefined physical post-processing to force CHSH. Instead, binning is used as a convergent numerical relaxation of the underlying infinite linear program: increasing the number of bins yields a hierarchy whose contextual fraction values monotonically approach the continuous optimum.

Our starting point is a recently proven CV version [25] of the Fine–Abramsky–Brandenburger theorem [26, 27], which shows that CV Bell non-locality is a specific in-

* carlos-ernesto.lopetegui-gonzalez@lkb.upmc.fr

† mattia.walschaers@lkb.upmc.fr

stance of contextuality [27]. This connection provides a well-defined quantifier of the amount of non-locality of a given experiment, via its contextual fraction [24]. The contextual fraction explains which fraction of the observed measurement statistics cannot be explained through a local hidden-variable model. It is equivalent to the maximal normalized Bell inequality violation possible with the available data. Both the value of the contextual fraction and the optimal Bell inequality can be obtained through a linear optimization program. In the CV setting, it becomes an infinite linear program, which cannot be solved exactly. In [25], a convergent hierarchy of relaxations of this infinite linear program was provided. This hierarchy consists of positive semidefinite optimization programs (SDP), based on the matrices of moments of the empirical data. However, after an in-depth numerical exploration of this approach, we find it to be unfruitful for detecting Bell non-locality in CV quantum experiments. In Appendix A, we present a description of the hierarchy and a discussion of our findings.

For this reason, we focus on a different relaxation of the infinite linear program to compute the contextual fraction. The relaxation is constructed by performing a fine-grained binning of the probability distributions of the measurement outcomes. This results in a hierarchy of finite linear optimization programs, whose results converge to the exact one by increasing the number of bins. In [25], it was proven that the contextual fraction decreases monotonously with such binning, which guarantees that a contextual fraction obtained for a finite number of bins provides a lower bound of the exact one. This approach allows us to develop a framework that, given access to experimental data, quantifies the amount of non-locality and provides the corresponding optimal Bell inequality.

Using our framework, we perform extensive numerical searches over potential CV experiments (testing both states and measurement settings), and confirm that binning strategies are in general optimal. We recover many existing results [14–16, 20], and find several new examples of CV Bell violations. Notably, for the first time, we find an example of a two-mode non-local CV experiment with homodyne measurements, whose non-locality cannot be detected through the CHSH approach, but requires a Bell inequality which is equivalent to the CGLMP Bell inequality for qutrits [28]. We also explore three-mode scenarios, for which we obtain contextual fractions well beyond the Tsirelson bound for CHSH [29], *i.e.*, the maximum contextual fraction that can be certified using a CHSH-like Bell inequality.

Moreover, our framework is agnostic to the dimension of the underlying physical system. This makes it an ideal tool for the study of hybrid DV-CV systems [30, 31], with the added value that the DV system can be treated exactly, while the CV part can be treated with a higher, controlled accuracy. We identify several simple hybrid quantum states for which a large contextual fraction can be obtained.

The rest of the paper is organized as follows. In section

II, we formalize the general setting with which we deal. In section III, we introduce the linear program which we implement. Later, in section IV, we present different examples of quantum states and measurement settings for which the program detects Bell non-locality. For each example, we present the corresponding optimal Bell inequality. Finally, in section VI, we discuss the implications of the results obtained and highlight interesting open questions.

II. MEASUREMENT SCENARIO

In this section, we present the general setting that we are dealing with. We make emphasis on the link between Bell non-locality experiments and the more general language of contextuality.

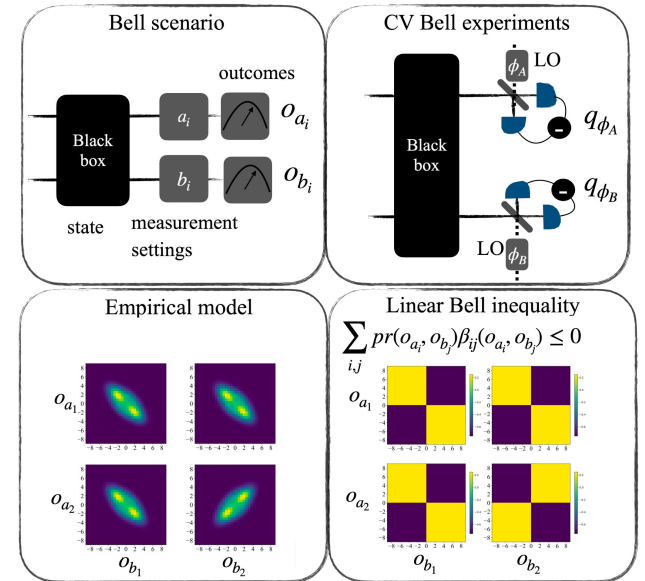


FIG. 1. Top left: description of a general Bell scenario for two parties. Each party performs a measurement among different available settings a_i (b_i), and obtain measurement outcomes o_{a_i} (o_{b_i}). Top right: continuous-variable Bell experiment. Each party performs a homodyne detection measurement, setting different quadrature measurements by tuning the phases φ_A (φ_B) of their local oscillators. Bottom left: The data obtained from this kind of experiment usually comes in the form of histograms of commuting variables, or contexts. The marginals of contexts sharing variables have to be consistent with each other. The set of all histograms provides an empirical model. Bottom right: We test each empirical model for Bell nonlocality (contextuality), and as a byproduct obtain the optimal Bell inequality for the given empirical model. The plots represent the distribution of values for the filters β_{ij} that parametrize the Bell inequality. For the specific example shown, the optimal Bell inequality is equivalent to sign binning followed by CHSH.

In Fig. 1, we present the general scheme for a Bell experiment over two parties. We consider the broader scenario of more than two parties, but represent only two

for clarity purposes. Alice and Bob each have access to a subsystem of a state $\hat{\rho}$, prepared in some black box, of which they have no information. Each of them can perform a measurement, chosen among different available settings $M_A = \{a_1, \dots, a_{n_A}\}$ and $M_B = \{b_1, \dots, b_{n_B}\}$ respectively. The main case of interest for us in this work is the case in which Alice and Bob perform homodyne measurements of the quadratures of a harmonic oscillator, for example the amplitude and phase quadratures of a mode of an electromagnetic field [10]. In this case, the different settings correspond to different choices of the measured quadrature, and the outcome space is continuous and unbounded, $o_{a_i(b_j)} \in \mathbb{R}$. Due to measurement incompatibility, the simultaneous measurement of different local settings is in general impossible, and the results of the experiment are the different probability densities (histograms) $p(o_a, o_b | a_i, b_j)$ for each possible pair of compatible measurements $\{a_i, b_j\}$. The non-signaling principle implies that for spatially separated experimenters the choice of measurement setting by one of them should not influence the statistics of outcomes observed by the other, *i.e.*,

$$\begin{aligned} p(o_a | a_i) &= \int_{\mathbb{R}} do_b p(o_a, o_b | a_i, b_j) \\ &= \int_{\mathbb{R}} do_b p(o_a, o_b | a_i, b_k), \end{aligned} \quad (1)$$

for all j, k . A similar expression can be written for different choices of measurements by Alice.

The central question in the analysis of Bell non-locality is to determine whether the statistics obtained from the experiment is consistent with local realism, which would imply that it can be described by some local hidden variable model (LHVM) of the form

$$p(o_a, o_b | a_i, b_j) = \int_{\Lambda} d\mu(\lambda) p(o_a | a_i, \lambda) p(o_b | b_j, \lambda), \quad (2)$$

where $\mu(\lambda)$ defines a probability measure for the hidden variable $\lambda \in \Lambda$. Notice that this assumes that all correlations observed in an experiment are of a classical nature, and the state vector description comes from a lack of knowledge about an underlying statistical process.

The question about the existence of an LHVM has been addressed either by methods that directly try to construct it or, in a more historical approach, through Bell inequalities [2, 32]. Convexity of the set of local behaviors, *i.e.*, of the set of experiments that could be described by an LHVM, guarantees that for every behavior outside this set, there is an inequality that can optimally discriminate it.

An equivalent description can be obtained through the lens of the broader concept of contextuality [27, 33]. The notion of contextuality that we deal with, due to Kochen and Specker [33], should not be confused with the preparation and measurement contextuality due to Spekkens [34]. The kind of settings considered by contextuality includes those in Fig.1, but it's not restricted to it. It can

include non-local measurements, or multiple local measurements. Any contextuality experiment is described by a measurement scenario $\langle X, \mathcal{M}, O \rangle$, where

- X is the set of measurement labels.
- \mathcal{M} is a covering family of subsets of X , *i.e.*, such that $\bigcup \mathcal{M} = X$. The elements $C \in \mathcal{M}$ of this set are called maximal contexts and are maximal sets of compatible observables.
- $O = (O_x)_{x \in X}$ specifies a measurable space of outcomes for each measurement x , $O_x = \langle O_x, \mathcal{F}_x \rangle$, where \mathcal{F}_x is a sigma algebra on O_x , *i.e.*, a family of open subsets of O_x .

This general definition of a measurement scenario allows to specify arbitrary experiments to probe contextuality in a broad sense. The description compatible with continuous variable Bell non-local experiments of the type described in Fig.1, is given by $X = \{a_1, \dots, a_{n_A}, b_1, \dots, b_{n_B}\}$, $\mathcal{M} = \bigcup_{i,j} \{a_i, b_j\}$, and $O_x = \langle \mathbb{R}, \mathcal{B}_{\mathbb{R}} \rangle$, where $\mathcal{B}_{\mathbb{R}}$ is the σ -algebra generated by all the open sets on the real line. Typically, we will consider O_x defined by a bounded subspace of the reals, which is consistent with the finite energy constraint of experiments.

The set of histograms that are accessible through the experiment, which we here call e_C to simplify the notation, define an *empirical model*, on the measurement scenario $\langle X, \mathcal{M}, O \rangle$. The non-signaling constraint is a specific instance of the compatibility condition $e_{C \cap C'}|_C = e_{C \cap C'}|_{C'}$, which implies that the statistics of subsets of a maximal context is independent of the remaining set of compatible measurements performed.

Definition 1. An empirical model $e = (e_C)_{C \in \mathcal{M}}$, on a measurement scenario $\langle X, \mathcal{M}, O \rangle$, is extendable (or non-contextual), if there is a probability measure μ on the space O_X , such that $\mu|_C = e_C$, for every $C \in \mathcal{M}$.

In the specific case that we consider, what this implies is that the measurement statistics obtained from the Bell experiment is non-contextual, if there is a probability distribution over all observables measured, $\mu(o_{a_1}, \dots, o_{a_{n_A}}, o_{b_1}, \dots, o_{b_{n_B}})$, such that, for every $\{a_i, b_j\}$,

$$p(o_{a_i}, o_{b_j}) = \int \prod_{k \neq i, l \neq j} do_{a_k} do_{b_l} \mu(o_{a_1}, \dots, o_{a_{n_A}}, o_{b_1}, \dots, o_{b_{n_B}}).$$

An empirical model that fails to be extendable, is called *contextual*. Notice that if a model is extendable, it implies that the same statistics could have resulted from an underlying stochastic process that samples all observables jointly. The contradiction between contextual assignments and global assignments of values to each observable is at the core of contextuality. In non-locality experiments, it turns out that the existence of a LHVM is equivalent to the existence of an extendable or non-contextual description [26, 27, 33]. A contextual empirical model in this case can equally be called Bell non

local. Recently, this connection was formally proven for continuous variable measurement scenarios [25].

As a consequence of this connection, it is possible to quantify the degree of non-locality through a well defined quantifier of contextuality, the contextual fraction [24, 25]. Intuitively the contextual fraction quantifies the portion of the data that cannot be *explained* through an extended probability distribution. An extendable model has a contextual fraction equal to zero. Conversely, we can define the non-contextual fraction, which is maximal, equal to 1, for extendable models. Formally it is defined as

Definition 2. The non contextual fraction associated to an empirical model e , $NCF(e)$ on a measurement scenario $\langle X, \mathcal{M}, O \rangle$, is given by

$$\sup\{\mu(O_x) | \mu \geq 0, \forall C \in \mathcal{M} : \mu_C \leq e_C\}.$$

Because all e_C are well defined probability distributions, the non-contextual fraction $NCF(e) \in [0, 1]$. The contextual fraction is defined as $CF(e) = 1 - NCF(e)$.

Phrasing the contextual fraction in terms of an optimization over a space of functions, allows to write a linear optimization program to compute it [24], which in the case of continuous variable systems is infinite [25]. In the following section we discuss the said program and its relaxations.

III. QUANTIFYING CONTEXTUALITY

Definition 2, allows to define a (possible infinite) linear optimization program to compute the (non)contextual fraction, as a well defined quantifier of (non)contextuality, and in turn of non-locality. The program can be written as

$$(P) \left\{ \begin{array}{l} \text{Find } \mu \in F_{\pm}(O_X) \\ \max \mu(O_X) \\ \text{s.t. } \forall C \in \mathcal{M} \mu|_C \leq e_C \\ \mu \geq 0. \end{array} \right. \quad (3)$$

where F_{\pm} represents the set of signed functions. The output of this program is the non-contextual fraction $NCF(e)$, associated to the empirical model e , over the corresponding measurement scenario. If a non-contextual model for $\{e_C\}$ exists, then μ will be a well defined probability distribution over O_X , and the output of the program will be a maximal non contextual fraction of 1. As for any optimization program, a dual can

be defined. In this case it is given by

$$(D) \left\{ \begin{array}{l} \text{Find } (f_C)_{C \in \mathcal{M}} \in \prod_{C \in \mathcal{M}} C_0(O_C, \mathbb{R}) \\ \min \sum_C \int_{O_C} f_C d e_C \\ \text{s.t. } \sum_C f_C \geq 1 \text{ on } O_X \\ \forall C \in \mathcal{M}, f_C \geq 0, \end{array} \right. \quad (4)$$

where $C_0(O_C, \mathbb{R})$ is the set of continuous functions over O_C , the outcome space for each context. As for the primal program, (D) returns the non contextual fraction. This program offers a direct way to recover a Bell inequality for the given empirical model, provided it is contextual. Under a change of variables

$$\beta_C = \frac{1}{|\mathcal{M}|} - f_C,$$

the dual program transforms into

$$(B) \left\{ \begin{array}{l} \text{Find } (\beta_C)_{C \in \mathcal{M}} \in \prod_{C \in \mathcal{M}} C_0(O_C, \mathbb{R}) \\ \max \sum_C \int_{O_C} \beta_C d e_C \\ \text{s.t. } \sum_C \beta_C \leq 0 \text{ on } O_X \\ \forall C \in \mathcal{M}, \beta_C \leq |\mathcal{M}|^{-1} \mathbf{1} \text{ on } O_C, \end{array} \right. \quad (5)$$

whose output is directly the contextual fraction of the empirical model. For a non contextual, extendable, empirical model, $\{e_C\}$ can be extended to some μ over O_X , which implies that

$$\sum_C \int_{O_C} \beta_C d e_C = \int_{O_X} d\mu \sum_C \beta_C \leq 0,$$

implying that the optimal value is zero. On the other hand, for a maximally contextual model, like a PR box [35, 36], there is an assigning strategy that allows to put $\beta_C(x_C) = 1/|\mathcal{M}|$, for every x_C for which $e_C(x_C) \neq 0$. This implies that the output of the program is

$$\sum_C \int_{O_C} \beta_C d e_C = \sum_C \frac{1}{|\mathcal{M}|} \int_{O_C} d e_C = 1,$$

which is indeed the maximum possible value of the contextual fraction. Moreover, any solution $\{\beta_C\}$, parametrizes a Bell inequality of the form

$$B(e_C) = \sum_C \int_{O_C} \beta_C d e_C \leq 0, \quad (6)$$

negative for any non-contextual (local) behavior. If on the other hand the empirical model is contextual and $CF(e) > 0$, then the set of functions β_C parametrize the optimal Bell inequality for the given empirical model.

The programs described in this section are all infinite linear programs, which cannot be solved exactly. Nevertheless, there are different ways of relaxing them into hierarchies of finite problems that incrementally approximate the solution of the infinite ones. In [25], a relaxation into a hierarchy of semidefinite program (SDP), based on the moments of the empirical distributions, was proposed. In appendix A, we present it for completeness. The Bell inequalities that can be obtained at any level of this hierarchy correspond to polynomial Bell inequalities, *i.e.*, all β_C in (6) are polynomials of the observables, and thus the Bell inequality can be evaluated in terms of the moments of the distribution, without need for discretization of the data. During the course of our work, as a first attempt to obtain genuinely CV Bell inequalities, we implemented the hierarchy of moment based SDPs. The implementation can be found on the GitHub repository [37]. After extensive numerical search, it was not possible to find any continuous variable empirical behavior for which a polynomial Bell inequality existed. Naturally, if we could probe arbitrarily high orders in the hierarchy we would find Bell inequalities at some point; yet, up to the limit which we could actually probe *i.e.*, polynomials of degree at most ~ 18 , no working example was found. On the other hand, as discussed in the appendix A, the program was able to obtain Bell inequality for non-physical empirical models like the continuous extensions of PR boxes, described in [36]. When optimizing over the set of quantum states, no state violated these Bell inequalities.

A different approach to relaxing the infinite LP is to approximate the continuous distributions as histograms, thus involving only an arbitrary discretization of the outcome space. This simply transforms the program into a finite linear program. We discuss the details of this program in the following subsection.

A. Finite version of the infinite LP

Formally, the objects involved in the finite program approximating the exact non-contextual fraction is obtained by binning the input distributions $\{e_C\}$ into histograms, as

$$E_C^{(i_1, \dots, i_M)} = \int_{O_C} e_C \theta_{i_1, \dots, i_M}(\vec{x}_C) d\vec{x}_C, \quad (7)$$

where M is the number of local parties, or equivalently, the number of measurements per context; and

$$\theta_{i_1, \dots, i_M}(\vec{x}_C) = \begin{cases} 1 & \text{if } x_{i_k} \in [x_d[i_k], x_d[i_k + 1]] \\ 0 & \text{otherwise.} \end{cases}$$

Here $x_d = \{-\infty, -A, -A + \delta, \dots, A - \delta, A, \infty\}$ represents the discretization of the real axis. Notice that a choice for A has to be made so that the probability mass left out is below some chosen threshold. A discussion about the implication of the choice of such a compact subset of the outcome space is discussed in section 6 in [25]. Beyond

the two extreme bins, the rest of the bins are spaced homogeneously between $-A$ and A , with a spacing $\delta = 2A/N_b$, with N_b the number of bins. For a given empirical model and binning choice, the primal program becomes

$$(P_{N_b}) \left\{ \begin{array}{l} \text{Find } \mu \in \mathbb{M}(N_b^{|X|}) \\ \max \sum_{i_1, \dots, i_{|X|}} \mu_{i_1, \dots, i_{|X|}} \\ \text{s.t. } \forall C \in \mathcal{M} \mu|_C \leq E_C \\ \mu \geq 0, \end{array} \right. \quad (8)$$

where all inequalities are element-wise. The dual program, directly written in terms of β_C , so that it returns the contextual fraction, can be written as

$$(B_{N_b}) \left\{ \begin{array}{l} \text{Find } (\vec{\beta}_C)_{C \in \mathcal{M}} \in \bigoplus_{C \in \mathcal{M}} \mathbb{R}^{N_b \times N_b} \\ \max \sum_C \sum_{i_1, \dots, i_M} \vec{\beta}_C^{(i_1, \dots, i_M)} E_C^{(i_1, \dots, i_M)} \\ \text{s.t. } \sum_C P_X(\vec{\beta}_C) \leq \vec{0} \text{ on } O_X \\ \forall C \in \mathcal{M}, \vec{\beta}_C \leq |\mathcal{M}|^{-1} \mathbf{1} \text{ on } O_C. \end{array} \right. \quad (9)$$

Any such program, for an arbitrary number of bins, provides a lower bound on the exact contextual fraction, which is already pointed out in [25] by proving that the contextual fraction is decreasing under classical processing like binning. On the other hand, to build up a well defined hierarchy of programs, with a monotonic convergence, we need to choose some way to incrementally smooth out from a rough discretization toward the continuous version, *i.e.*, we need to parametrize the way in which we increase the number of bins. We can choose to do it by first fixing A , which can be done without loss of generality as long as we make sure to leave only an $\epsilon \ll 1$ fraction of the data outside, with the guarantee of an error $\mathcal{O}(\epsilon)$ on the contextual fraction [25]. We can then choose $N_b(k) = 2^k$, it is, each time we double the number of bins. This guarantees that $E_{C,k-1}$ can be obtained from $E_{C,k}$ by coarse-grain. For the hierarchy to be sound, the following two statements have to hold,

1. $\forall k \in \mathbb{N}^+$, we have $CF_k \geq CF_{k-1}$;
2. $\lim_{k \rightarrow \infty} (CF_k) = CF$.

Here CF_k is the contextual fraction obtained at level k in the hierarchy, *i.e.*, by solving B_{2^k} . The proof in section 5.2 of [25], for the monotonicity of the contextual fraction under binning as a classical operation directly implies that the two statements above hold.

Before proceeding to present the results that we obtain by implementing this hierarchy of programs, there are several points to discuss. First, the technical implementation of the hierarchy is restricted because of computational limitations, with some strict constraints imposed by the number of parameters that optimization program solvers can handle. In our implementation, which can be

found in [37], this limits, in the case in which Alice and Bob each perform two measurements, to a maximum of 214 bins per quadrature, *i.e.*, to level $k = 7$ on the hierarchy (128 bins). For a case in which we deal with three modes and two measurements, the limit is around 32 bins, as well as for three measurements per party in a two parties experiment. This being said, for the case of two parties and two measurements per mode, the description is sufficiently fine grained to recover all the smooth features in the empirical distributions, and as such, to recover any smooth features that there could be in an optimal Bell inequality. Moreover, the functions β_C that parametrize the Bell inequalities are not constrained to specific values, but can take any arbitrary value as long as they collectively satisfy the constraints on the program. This is a radically different approach to all previous attempts to find linear Bell inequalities for CV systems [12–16, 18, 20]. In section IV we discuss several examples of states and measurements for which the hierarchy succeeds in finding the optimal Bell inequality.

Furthermore, the hierarchy of programs defined in this section offer a powerful tool to deal with hybrid DV-CV experiments. It allows to treat exactly the DV system, while focusing all computational resources on the CV one. For instance, if we consider a qubit system for the DV part, there is practically no constraint on the number of bins to consider on the CV side. In section V we discuss several examples of hybrid states that could lead to a very large Bell inequality violation with homodyne detection on the CV side and Pauli measurements on the DV side.

IV. RESULTS FOR CONTINUOUS-VARIABLE SYSTEMS

In contrast to what happens when we work with the moment based SDP, the finite linear program succeeds in detecting contextual behaviors in several quantum states, without needing to go too high in the hierarchy defined in section III. In this section we present several examples of quantum states of bosonic systems for which we are able to find the optimal Bell inequalities. First, we show that for many empirical scenarios considered previously in the literature of CV Bell inequalities, the optimal Bell inequalities are parametrized by dichotomic functions, which, up to some normalization are equivalent to the binary strategies used in the respective papers. Then we show some other examples of two-mode entangled states for which we found optimal Bell inequalities. Notably, among those examples, there is one for which the optimal Bell inequality cannot be mapped in any way to CHSH, but, for the first time in the CV literature, is equivalent to the qutrit version of the CGLMP Bell inequality [28]. Finally, we show a multimode state for which a significant contextual fraction is obtained, beyond the Tsirelson bound for the CHSH Bell inequality [29].

A. All previously identified binary strategies are essentially optimal

In what follows, we briefly discuss several examples previously considered in the literature for violating Bell inequalities with homodyne detection. Despite searching for optimal Bell inequalities for all cases, in an automatic way, no improvement over the previous results was found for any of these cases, after normalizing the Bell inequality so that its maximum value is 1.

1. Photon subtracted states

In [15, 16], García Patrón et al. proposed a scheme for violating Bell inequalities with photon-subtracted states [38], using homodyne detection statistics. They employ the CHSH inequality, after sign binning the outcomes of the homodyne detection. That is, if Alice measures a quadrature q_A^φ , then she will record the value $a_\varphi = \text{sign}(q_A^\varphi)$.

We probed a similar setup with the aim of finding the optimal Bell inequalities for the settings they considered. It turns out that, as will be shown below, the strategy employed in [15, 16] is the optimal one. This claim was conjectured in the paper based on numerical explorations and analysis of the features observed on the probability distributions.

We consider the following family of states

$$|\psi\rangle = (\hat{a}_1 \cos \theta + \hat{a}_2 \sin \theta) \hat{a}_1 \hat{O}(\pi/4) S_1(r_1) \hat{S}_2(r_2) |0\rangle, \quad (10)$$

where $\hat{O}(\pi/4)$ represents a balanced beam splitter operation, $\hat{S}_i(r_i)$ represents the single mode squeezers [10], and \hat{a}_i stand for the annihilation operator corresponding to each mode [39]. In Fig.2 we can observe the behavior of the contextual fraction for these states, as the mode on which the second photon is subtracted is changed, according to the parameter θ . This allows to interpolate between the case in which both photons are subtracted on the same mode $\theta = 0$, and the one in which they are subtracted in complementary modes $\theta = \pi/2$. The results obtained for those extreme cases coincide with those reported in [15, 16]. There, the Bell value for the CHSH for the case of $\theta = \pi/2$ is $B = 2.046$, which corresponds to a fractional violation $\mu = \frac{B-2}{B_M-2} = 0.023$, which is similar to the value obtained by us. The plot is constructed using $r_1 = -r_2 = 0.68$, which provides the maximum Bell violation in [15, 16].

In Fig.3 we can observe the empirical distributions for which the maximum contextual fraction was obtained. Alongside we show the *filter* functions β_C , that parameterize the corresponding Bell inequality. We can see that the distributions carry large resemblance with PR distributions, and thus the corresponding Bell inequality is the same. Such filters precisely correspond, after some renormalization steps, to the sign binning procedure employed in [15, 16], which is thus optimal, as they had

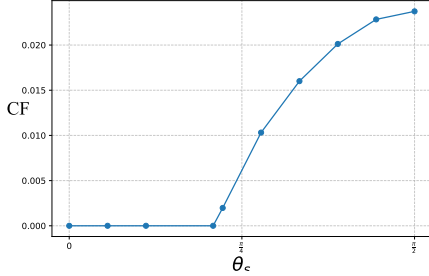


FIG. 2. Contextual fraction associated to the measurement statistics of two photon subtracted states from the family described in equation (10). In all cases, a search was performed over different configurations of the homodyne detector settings to obtain the maximum contextual fraction possible. For all the non-zero values, they correspond to measuring $\varphi_1 \in \{0, \pi/2\}$ and $\varphi_2 \in \{-\pi/4, \pi/4\}$.

conjectured.

Several other examples of two photon subtracted states were considered, without major improvement over the figures described in [15, 16]. Moreover, we explored the case of three photon subtraction, for which no Bell inequality violation was reported in that paper, and we were not able to find any numerically significative contextual fraction. The fact that specifically three photon subtractions not only do not increase the contextual fraction for homodyne measurements, but actually reduce it zero, is a rather counterintuitive result, for which we do not have an explanation.

2. Multi-peak states

In what follows we consider complex multi-peak states, described in [14]. Several states were considered in that paper, of the form

$$|\psi\rangle = \frac{|ff\rangle + e^{i\pi/4}|gg\rangle}{\sqrt{2}}, \quad (11)$$

where $|f\rangle, |g\rangle$ are two orthogonal (or approximately orthogonal) state vectors. A finite photon number state was considered as one of the approximations, taking:

$$\begin{aligned} |f\rangle &= \sqrt{0.459}|0\rangle - \sqrt{0.491}|4\rangle - \sqrt{0.008}|8\rangle - \sqrt{0.042}|12\rangle \\ |g\rangle &= \sqrt{0.729}|1\rangle + \sqrt{0.155}|5\rangle - \sqrt{0.107}|9\rangle - \sqrt{0.009}|13\rangle. \end{aligned} \quad (12)$$

In Fig.4, we can observe the empirical behavior and the Bell filters obtained through the implementation of the linear program. The contextual fraction obtained was 0.404, remarkably close to the Tsirelson bound [29]. Moreover this value is similar to the value obtained in the paper where the state was proposed, implying that the Bell inequality used was optimal, and coincides with the Bell inequality parameterized by the filter functions β_C

in Fig.4. Further simplifications of the states described above, with smaller number of photons, which were already discussed in [14], still provide a significant contextual fraction. Such states could be produced in the lab, using boson sampling like strategies, following the results in [40].

Other finite photon number states, as those considered in [20] were explored, yielding again similar results as those reported by relying on CHSH based strategies. In what follows we report the results of our own exploration for states and settings providing significant non-zero contextual fraction.

B. Finding needles in the haystack

As it turns out, finding states that display non-locality under homodyne detection, and in particular for the case in which each party is allowed to make two measurements, is complicated. The search for such states involve a search over a huge parameter space. One would be tempted to think of this as an optimization problem: we could define a parameterized family of states and search for the one(s) providing the largest contextual fraction. But the caveat is on the fact that the landscape is mostly flat, i.e., for most states the contextual fraction is zero. This makes it impossible to find good directions to move along in the parameter space. In other words, we are looking for a needle in a haystack.

That being said, it is still possible to find interesting states. Notably, bosonic codes, *i.e.*, CV states used to encode qubits, offer an interesting proxy to search for Bell inequality violations. Among those codes, GKP states [41], are particularly well suited to find Bell inequalities based on homodyne detection, given that Pauli measurements on them are performed by homodyne detection. The Pauli Z measurement is performed through measuring the amplitude quadrature q , while the X is performed by measuring the phase quadrature p . On the other hand, non-Pauli measurements, like $\cos \theta X + \sin \theta Z$ require non-linear operations before performing homodyne detection, which we do not allow for in our measurement scenarios.

To find a GKP entangled state that should violate a Bell inequality by measuring only amplitude and phase quadratures, we thus find the equivalent qubit entangled state that should violate the CHSH Bell inequality for only Pauli measurements X, Z (other states could be constructed if other combinations of Pauli measurements were considered). Such a state is

$$|\psi_{qubit}\rangle = \frac{(|11\rangle - |00\rangle - (1 + \sqrt{2})(|01\rangle + |10\rangle))}{2\sqrt{2 + \sqrt{2}}}. \quad (13)$$

The equivalent CV state can be obtained by replacing the code words $|0\rangle, |1\rangle$, by approximate GKP states. We approximate GKP states by weighted superpositions of displaced squeezed vacuum states. For the moment we do not place much concern on the form of the envelope

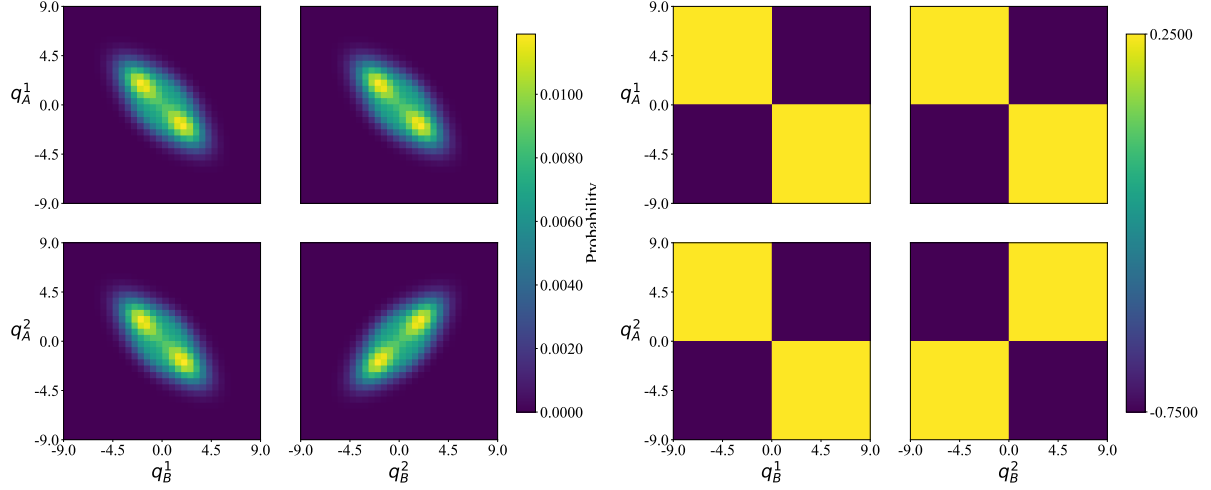


FIG. 3. On the left the empirical distribution corresponding to the homodyne statistics obtained by measuring settings $\varphi_A \in \{0, \pi/2\}$ and $\varphi_B \in \{-\pi/4, \pi/4\}$, on a two photon subtracted state, from the family described in equation (10). This corresponds to the case $r_1 = -r_2 = 0.68$, $\theta = \pi/2$. On the right: the *filter* functions, β_C , that define the optimal Bell inequality for the empirical model considered.

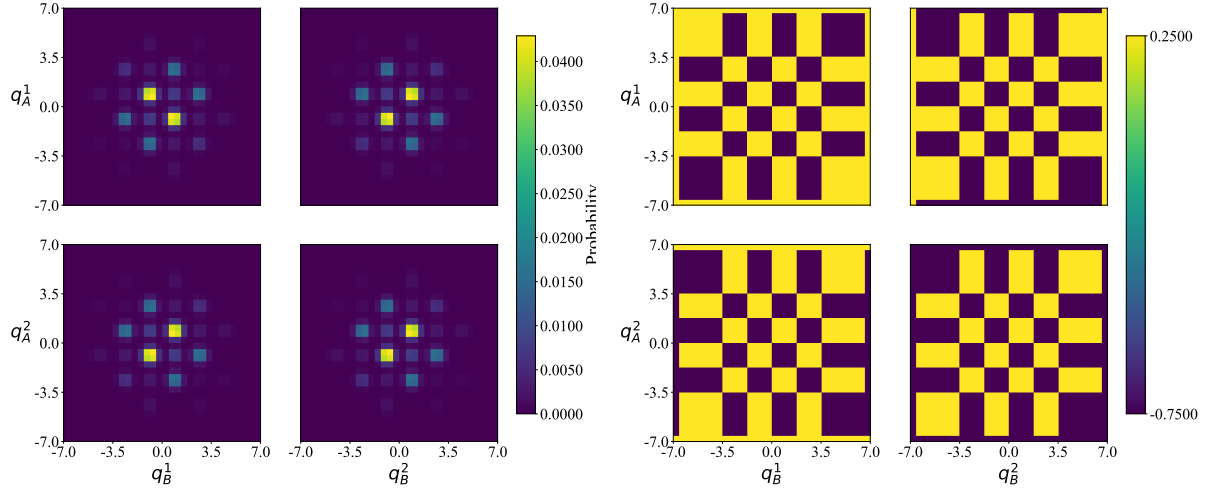


FIG. 4. On the left the empirical distribution corresponding to the homodyne statistics obtained by measuring settings $\varphi_A \in \{0, \pi/2\}$ and $\varphi_B \in \{0, \pi/2\}$, on the state described jointly by equations (11) and (12). On the right: the *filter* functions, β_C , that define the optimal Bell inequality for the empirical model considered.

governing the decay of the weights, as the main focus is to find minimal working examples. With that in mind we first considered a state with five peaks to approximate the $|0\rangle$ qubit, and a state with six peaks to approximate the $|1\rangle$. We consider the spacing between peaks to be $\alpha = \sqrt{2\pi}$ and the squeezing of each peak to be $r = 0.9$. The states are plotted in Fig.5.

The joint quadrature distributions corresponding to joint measurements of amplitude or phase quadrature by the two different parties are presented on the left of Fig.6.

To the right of the figure we find the filters parameterizing the optimal Bell inequality for this empirical behavior. The figure is made with 64 bins per quadrature, a value for which the contextual fraction obtained was $CF_{GKP} = 0.3685$, meaning that 36.85% of the data cannot be explained by a non-contextual model. Considering only 32 bins the value obtained was 0.3452, for 16 bins it was already 0.2434, whilst 8 bins were not enough to capture the contextual behavior.

Even though the GKP states of Fig.5, inserted in

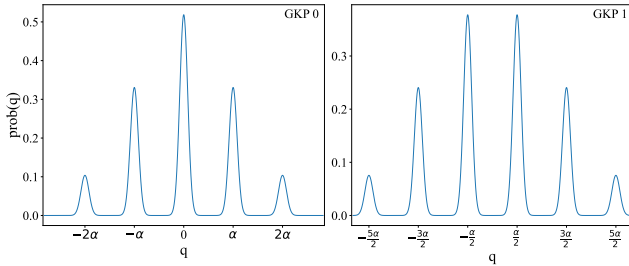


FIG. 5. Probability densities for the q quadrature of the GKP code words used to approximate the state in (13).

(13) provide a significant contextual behavior under a straightforward measurement scenario, such a state is very hard to engineer. In particular, in optical experiments, the best states reported thus far, on the single mode level, have no more than 3 peaks, with very small inter peak resolution [42]. On the other hand, those states may be more easily realizable on other experimental platforms with access to higher non-linearities [43–46]. Nevertheless, for this kind of experiments fast and efficient homodyne detection remains a challenge, with recent advances in superconducting platforms still far from the performance required for a Bell experiment [47]. The only other alternative would be to perform the full tomography of the state and obtain the marginals for our quadratures of interest, but this would no longer amount to a proper Bell experiment.

This forces us to ask the question whether we can find simpler approximations of the state that still lead present a significant amount of non-locality. For this we considered the simpler versions of the code-words given by

$$\begin{aligned} |0\rangle &= \hat{S}(r)|0\rangle_b \\ |1\rangle &= \frac{\hat{D}(\alpha) + \hat{D}(-\alpha)}{\sqrt{2}} \hat{S}(r)|0\rangle_b, \end{aligned} \quad (14)$$

where $|0\rangle_b$ corresponding to the vacuum state of the bosonic field; $\hat{S}(r)$ is the squeezing operator, and $\hat{D}(\alpha)$, the displacement operator, that implements a displacement by α along the amplitude quadrature ($\alpha \in \mathbb{R}$). The fact that these states are separately easy to prepare in optical experiments (depending on the value of α), does not imply that preparing the final entangled state (13) is a simple task, but it is a more reasonable first step than preparing the highly multipeak states of Fig.5.

In Fig.7 we can observe the joint statistics for the joint measurements of phase and amplitude quadratures. To the right of the figure, the Bell filters β_C that parametrize the optimal Bell inequality for this empirical behavior. The contextual fraction obtained was $CF_{cat} = 0.262$, thus meaning that 26.2% of the data is not explainable with a local hidden-variable model. In Fig.8, we can observe the behavior of the contextual fraction under the effect of losses, when both modes suffer the same amount of loss. We can observe that a non-zero contextual fraction is observed up to around 15% losses, which is within

the range of state-of-the-art experiments. Note that we consider an ideal preparation and only apply losses subsequently, depending on the actual realistic preparation scheme of (13), the performance may differ (but this is beyond the scope of this article).

C. “Qutrit” GKP entangled states

Motivated by the qudit Bell inequalities in [28], we tried to find a family of bosonic states for which a Bell inequality with more than two values would be required, thus going beyond CHSH. For constructing the states we followed a similar strategy as outlined in the previous section for the qubit case. The CGLMP Bell inequality in [28] is provided in a way which is consistent with the treatment in finite LP program introduced in section III. It is thus not provided in operator form. We could nevertheless obtain the explicit operator form of the inequality, as a polynomial Bell inequality, using the SDP in A, which is also well suited for DV settings. After obtaining the polynomial Bell inequality, we optimize it for the case in which both parties perform generalized Pauli X and Z measurements. The resulting state involves a non-trivial superposition of the qutrit code words. The exact form of the state can be found in Appendix B, where we outline the derivation of the exact form of the state.

To construct an equivalent bosonic state we consider a GKP qutrit state encoding, which was also proposed on the original paper [41]. The codewords used are represented in Fig.9. The states are built of superposition of squeezed states with $r = 1$, which corresponds to around 10dB per peak, and a spacing of $\alpha = \sqrt{3\pi}$.

Using these states as codewords we generate an entangled state according to the description presented in appendix B. We consider the case in which both Alice and Bob perform measurements of the amplitude and phase quadratures (q and p). The corresponding empirical model can be observed to the left of Fig.10. On the same figure, to the right, there is the plot for the choices of β_C that parameterize the optimal Bell inequality found by the program for the given empirical model. The plots are done using 64 bins per quadrature, which is enough to capture all the relevant features of the distribution. The contextual fraction observed is around 25.4%. Using a smaller number of peaks still leads to a significant violation.

The Bell inequality encoded by the filters plotted in Fig.10 offer, for the first time, a practical Bell inequality for CV states that is not equivalent to CHSH. It is, nevertheless, equivalent to another discrete Bell inequality, the CGLMP qutrit Bell inequality presented in [28]. This again highlights an apparent discrete structure of Bell non-locality in CV systems under homodyne detection.

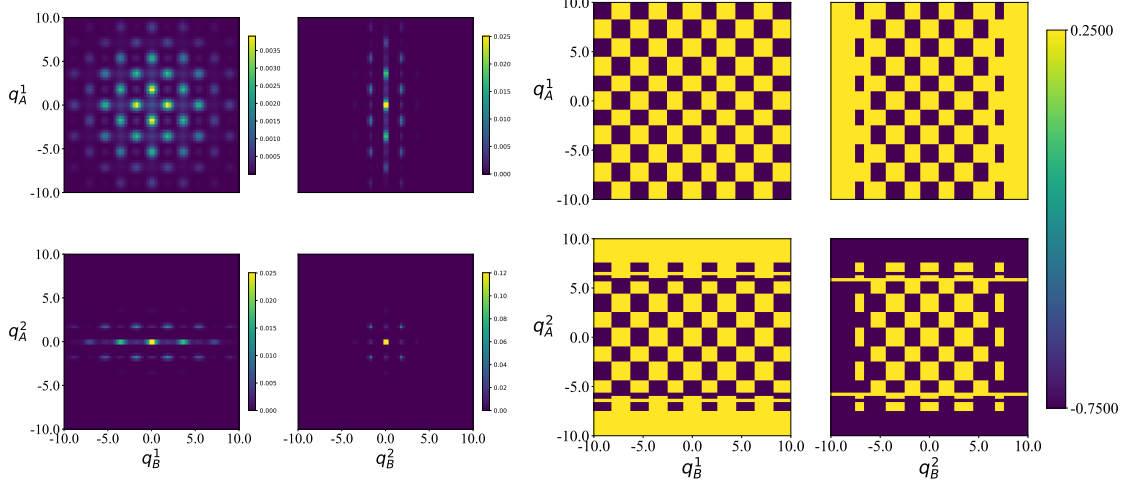


FIG. 6. To the left: joint histograms corresponding to the empirical model given by the homodyne settings $\varphi_A, B \in \{0, \pi/2\}$, on an entangled GKP state, given by equation (13). The approximate code-words are given by superposition of 5 and 6 displaced squeezed states, for the $|0\rangle$ and $|1\rangle$ states respectively. To the right: Filter functions β_C that parameterize the optimal Bell inequality for the empirical model at hand.

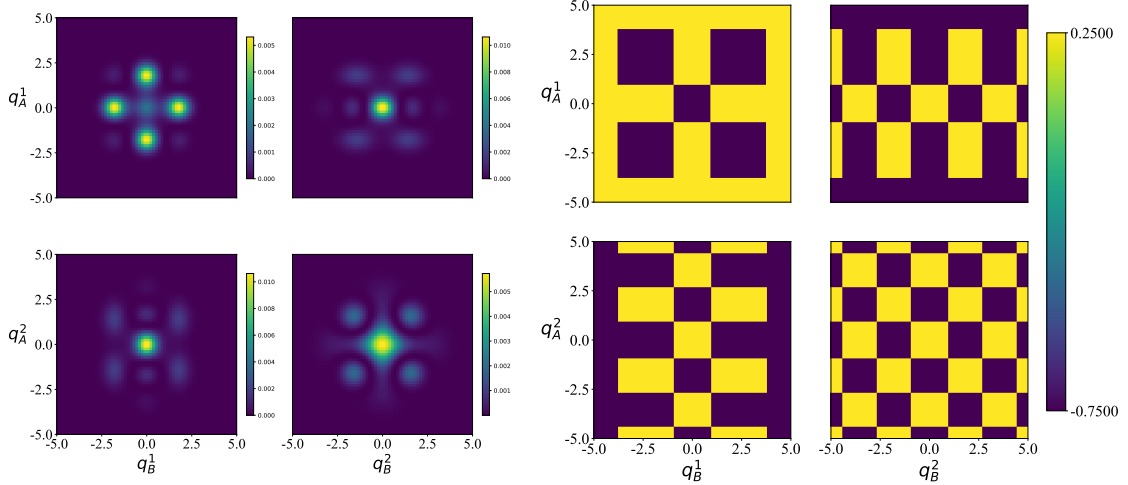


FIG. 7. To the left: joint histograms corresponding to the measurement scenario given by the homodyne settings $\varphi_A, B \in \{0, \pi/2\}$, on an entangled GKP state, given by equation (13). The approximate code-words are defined in equation (14). To the right: Filter functions β_C that parameterize the optimal Bell inequality for the empirical model at hand.

D. Multimode experiments

Considering multimode scenarios with the tools we have developed suffers from a limitation in computational power, that makes it impossible to consider a very fine-grained binning of the histograms. In particular, if we consider three modes, and two measurements per mode, it becomes very hard to consider more than 16 bins. On the other hand, as we will show in this section, 16

bins suffice to capture a very large contextual behavior in properly chosen states.

In this section again, we follow a similar rationale as in the previous ones. In [24], the emergence of contextuality on GHZ states [48] was discussed. In particular, they show that the empirical model obtained by performing Pauli X and Y measurements on each party of a GHZ

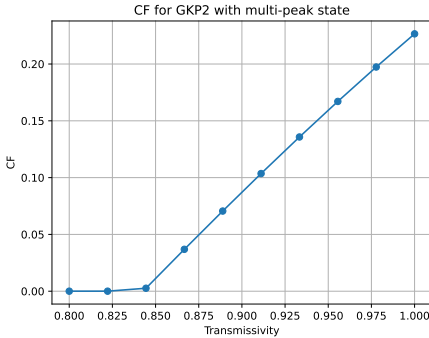


FIG. 8. Behavior of the contextual fraction under the effect of losses, for the empirical model defined by measurement of position and momentum quadrature of an entangled GKP state, with code words defined according to equation (14). On the x axis we plot the transmissivity of the channel, thus implying that the contextual behavior survives up to around 15% losses. Notice that we consider a symmetric loss channel, where both modes undergo the same amount of losses.

state

$$|\text{GHZ}_3\rangle = \frac{|000\rangle + |111\rangle}{\sqrt{2}}, \quad (15)$$

is maximally contextual, *i.e.*, the contextual fraction is 1. Moreover, in [18], they consider three mode GHZ states on a CV regime, encoded with even and odd cat states. In that case, they obtain a violation that is equivalent to a contextual fraction of around 10%. We consider here a similar construction, but pick the encoded states to be approximated GKP code words. We consider, to begin with, code words with 3 peaks and 2 peaks, with a spacing of $\sqrt{2}\pi$ and a squeezing per peak of $r = 1$. On each mode, we perform homodyne measurements of the p quadrature and of the quadrature $\frac{p+q}{\sqrt{2}}$. A modular measurement of these quadratures reproduce respectively Pauli X and Pauli Y measurements on the GKP encoding. Under this measurement scenario, we are able to certify a 60.5% contextuality on the resulting empirical model. We do this while considering only 16 bins per quadrature. If a larger number of bins could be considered, a larger contextual fraction would probably be obtained. Nevertheless, this suffices to witness contextuality that is higher than it is possible to observe with CHSH inequalities, for which the limit is $\sim 41\%$.

In the case of multimode Bell inequality, no direct observation of the histograms or Bell inequalities is possible, other than by flattening over some directions, or showing different projections. In any case, all the Bell inequalities obtained correspond to variations of the same binning strategies that have been discussed in previous sections. For a direct handling of the inequalities we refer to the implementation of these examples on the GitHub repository [37].

Using a similar encoding to that used for the two mode GKP entangled state, with a cat state encoding the qubit

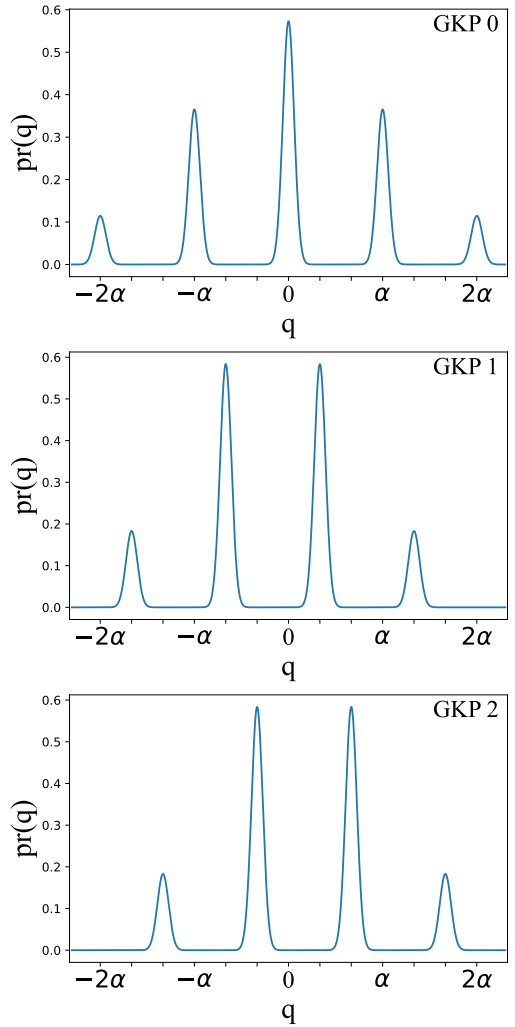


FIG. 9. Probability densities for the q quadrature of the GKP code words used to approximate a qutrit entangled state.

state $|1\rangle$ and a squeezed state encoding the $|0\rangle$, a contextual fraction of 8.5% is obtained.

V. RESULTS FOR HYBRID SYSTEMS

Hitherto we have explored experimental scenarios in which all parties involved are described in a continuous variable setting, and homodyne detection is performed on them. Nevertheless, the approach that we have developed is completely agnostic to the actual measurements performed, and is ideal to deal with observables with discrete outcomes. It is specially well suited for studying hybrid systems, which are composed of both DV and CV constituents [30]. The relevance of this kind of systems for quantum information processing has increased over recent years [30, 31, 49–51], for its relevance to developing interconnections between distant quantum devices, or for modular quantum computation.

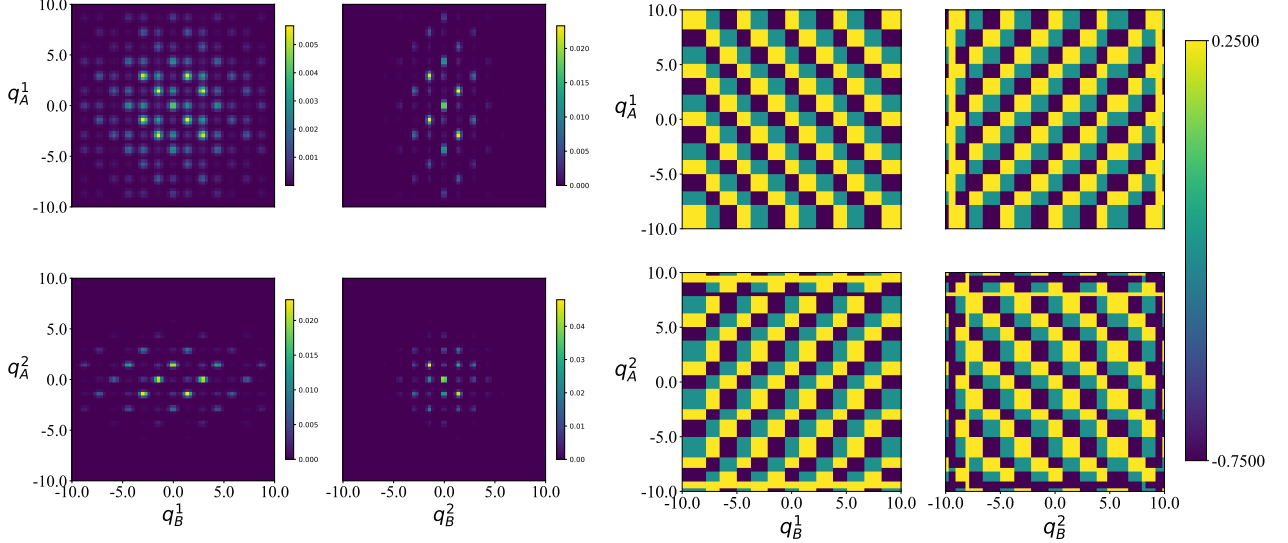


FIG. 10. To the left: joint histograms corresponding to the measurement scenario given by the homodyne settings $\varphi_A, B \in \{0, \pi/2\}$, on an entangled GKP qutrit state, according to the description in appendix B. The approximate code-words are plotted in Fig.9. To the right: Filter functions β_C that parameterize the optimal Bell inequality for this empirical model. A contextual fraction of 25.4% was obtained for this empirical model.

The analysis that we perform is platform independent, in the sense that we will consider the DV subsystem in an arbitrary way, assuming that we can perform arbitrary measurements on the Bloch sphere. This allows us to consider simpler states than we considered on the bosonic setup, given that we do not require to maximize Bell inequalities violations specifically for Pauli measurements. In particular, the Bell state

$$|\psi\rangle = \frac{|0\rangle_{DV}|0\rangle_{CV} + |1\rangle_{DV}|1\rangle_{CV}}{\sqrt{2}}, \quad (16)$$

maximize the CHSH Bell inequality when measuring $\{\frac{X+Z}{\sqrt{2}}, \frac{X-Z}{\sqrt{2}}\}$ on one side and $\{X, Z\}$ on the other side. This motivates the use of a GKP encoding on the CV side. The probability distribution for any pair of observables will be then an object of dimension $(2, N_b)$, where N_b is the number of bins used to discretize the quadrature statistics of the bosonic part. The wave vector associated to a pair of observables \hat{A} on the qubit part and \hat{q}_θ on the bosonic side, is given by

$$\psi(a, q) = \frac{\langle a|0\rangle_{DV}\psi_0(q|\theta) + \langle a|1\rangle_{DV}\psi_1(q|\theta)}{\sqrt{2}}, \quad (17)$$

where $|a\rangle$ is the eigenvector of \hat{A} corresponding to the outcome (eigenvalue) a ; and $\psi_n(q|\theta)$ are the wave functions of the arbitrary bosonic state encoding $|n\rangle$, along the quadrature \hat{q}_θ . Expression (17) is generally easy to compute and we can, from it, construct the distributions that define the empirical model to probe Bell non-locality.

We consider three different examples for the bosonic encoding, which are shown in Fig.11. First, we consider the same codewords as in Fig.5. Then we consider the same codewords as in equation (14), *i.e.*, a squeezed vacuum state encoding the $|0\rangle$, and a squeezed cat state for the $|1\rangle$. Finally, we consider to encode the states as even and odd squeezed cat states, given by

$$\begin{aligned} |0\rangle_{CV} &= \frac{|\alpha, r\rangle + |-\alpha, r\rangle}{\mathcal{N}(\alpha, r)} \\ |1\rangle_{CV} &= \frac{|\alpha, r\rangle - |-\alpha, r\rangle}{\mathcal{N}(\alpha, r)}, \end{aligned} \quad (18)$$

where $|\pm\alpha, r\rangle = \hat{D}(\pm\alpha)\hat{S}(r)|0\rangle$, is a displaced squeezed state. We consider $\alpha = \sqrt{2}\pi$, $r = 0.9$. All of these examples produce empirical models with a significant contextual fractions. For the specific parameters considered the values are 40%, 34.1% and 15.6% respectively. A detailed analysis of the resilience of these values to different experimental imperfections is left for future works.

VI. DISCUSSION AND OUTLOOK

On a technical level, our approach has the strength of being general, suitable for dealing with experimental data, and agnostic to the details of the underlying physics of the system. However, the scaling of our implementation with the number of modes is currently a bottleneck. Given the limitations of commonly used solvers like MOSEK, if we want to study four modes, we can-

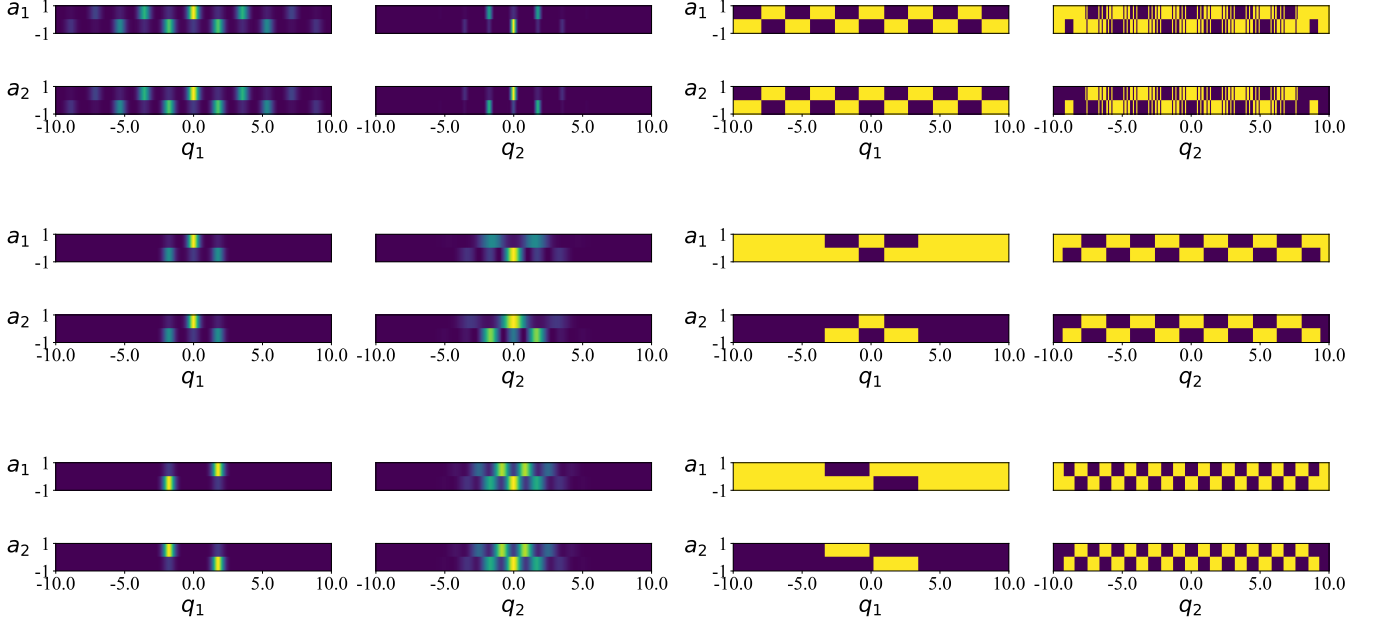


FIG. 11. From top to bottom the three different empirical models considered for probing Bell non-locality on hybrid DV-CV systems, according to the measurement scenario described in the main text. To the left there are all the histograms that define the corresponding empirical models. To the right, the filter functions β_C that parametrize the optimal Bell inequality for each case. From top to bottom, contextual fraction values of 40%, 34.1% and 15.6% were obtained. All color bars were omitted as it is the features of the histograms and Bell inequalities that are most relevant for us.

not consider more than ten bins per quadrature. This is a considerable limitation if we want to study CV systems. For DV systems, or hybrid systems, the scaling improves significantly. Notably, for qubit systems, up to 32 qubits can be considered. An alternative to such discretization schemes was provided by the moment based approach from [25], nevertheless, as we already discussed it does not seem to capture, within the order of moments that we can efficiently consider, the non-local behaviors. Yet, we cannot fully exclude the possibility of finding a similar decomposition technique, that could reduce the dimensionality of the problem and capture the non-local behaviors. Studying coarse-grained observables, like one does in spin systems [52] may provide a possibility to increase scalability.

Beyond the technical interest that the results obtained in this work may bear, they offer many interesting new insights into the non-locality of homodyne-detection-based experiments. In particular, our results force us to pose serious questions about the existence and relevance of a genuinely continuous type of non-locality. Throughout all the examples that we have explored, a common feature has emerged on all the optimal Bell inequalities: they are parametrized by discrete functions, *i.e.*, functions that evaluate to a finite number of values (2 or 3 in the cases we found). All the behaviors obtained can thus be simulated by experiments on discrete-variable systems. This hints at a discrete nature of homodyne-based non-

locality. Given the extensive numerical search that we have performed, we conjecture that this may indeed be a general fact. However, as we have no formal proof, this clearly provides an interesting open question for further research. Were this to be the case, it could potentially have implications on CV quantum information processing. The results that we have discussed may provide interesting information to tackle the question of whether multimode-CV systems offer a computational model that can go beyond the discrete ones.

Given that in all the examples considered the contextual fraction was never increased by adding more than two homodyne settings per mode, we can furthermore conjecture that no advantage can be obtained from considering larger numbers of settings. We have not been able to prove (or disprove) this claim, and we leave it as an open question.

In our examples, we have managed to achieve high contextual fractions, particularly, in the setting with more than two modes. We have seen cases where up to 60% of the measurement statistics could not be explained with a local hidden-variable model. Yet, it is natural to wonder whether there is, in principle, a non-trivial upper bound to the contextual fraction that can be reached in experiments with homodyne detection. In measurement setting that are equivalent to CHSH, we naturally recover a maximal contextual fractions of 41%, which corresponds to the Tsirelson bound. However, the CV setting is in

principle much more general, which makes it appealing to try and reinterpret these bounds through the lens of contextuality.

Overall, the search for states and homodyne measurement settings that provide non-local behavior has proven intensive, and in many ways feels like looking for a needle in a haystack. This implies that some states may have potentially been overlooked in our search. Our results provide a powerful new tool to be used in this kind of systematic searches, but it also highlights that there is still a significant lack of understanding of CV non-locality.

Because Bell nonlocality can be formulated as contextuality for Bell measurement scenarios, the study of CV contextuality may also increase our understanding of CV nonlocality. However, we must emphasize that resource characterizations of contextuality does not automatically transfer to Bell nonlocality. In particular, equivalences between contextuality and Wigner-function negativity established for broader measurement sets do not directly imply an analogous criterion for Bell nonlocality under local homodyne measurements. Indeed, Wigner negativity can occur even for separable states (e.g. Werner-type mixtures built from non-Gaussian components), showing that negativity is not sufficient for Bell nonlocality. Thus, connecting Bell nonlocality to other physical re-

sources remains an open challenge in the CV setting.

ACKNOWLEDGEMENTS

We acknowledge fruitful discussions with Robert Booth, Damian Markham, Lucas Porto and Antonio Acín. C.E.L.G. and M.W. acknowledge support through the ANR JCJC project NORDIC (ANR-21-CE47-0005). C.E.L.G., M.W., and F.G. were supported by Plan France 2030 through the project OQuLus (ANR-22-PETQ-0013). U.I.M. was supported by Plan France 2030 through the project EPiQ (ANR-22-PETQ-0007). E.O and G.M. acknowledge funding by the French national quantum initiative managed by Agence Nationale de la Recherche in the framework of France 2030 through the projects DIQKD (ANR-22-PETQ-0009) and QCommTestbed (ANR-PETQ-0011). U.C. and M.W. acknowledge funding from the European Union's Horizon Europe Framework Programme (EIC Pathfinder Challenge project Veriquib) under Grant Agreement No. 101114899. F.C. acknowledges funding from the European Union (EQC, 101149233). U.I.M and F.G. acknowledge funding from the European Union's Horizon Europe Framework Programme (CLUSTEC) under Grant Agreement No. 101080173.

[1] A. Einstein, B. Podolsky, and N. Rosen, *Phys. Rev.* **47**, 777 (1935).

[2] J. S. Bell, *Physics Physique Fizika* **1**, 195 (1964).

[3] A. Aspect, J. Dalibard, and G. Roger, *Phys. Rev. Lett.* **49**, 1804 (1982).

[4] M. Giustina, M. A. M. Versteegh, S. Wengerowsky, J. Handsteiner, A. Hochrainer, K. Phelan, F. Steinlechner, J. Kofler, J.-A. Larsson, C. Abellán, W. Amaya, V. Pruneri, M. W. Mitchell, J. Beyer, T. Gerrits, A. E. Lita, L. K. Shalm, S. W. Nam, T. Scheidl, R. Ursin, B. Wittmann, and A. Zeilinger, *Phys. Rev. Lett.* **115**, 250401 (2015).

[5] B. Hensen, H. Bernien, A. E. Dréau, A. Reiserer, N. Kalb, M. S. Blok, J. Ruitenberg, R. F. L. Vermeulen, R. N. Schouten, C. Abellán, W. Amaya, V. Pruneri, M. W. Mitchell, M. Markham, D. J. Twitchen, D. Elkouss, S. Wehner, T. H. Taminiau, and R. Hanson, *Nature* **526**, 682 (2015), publisher: Nature Publishing Group.

[6] L. K. Shalm, E. Meyer-Scott, B. G. Christensen, P. Bierhorst, M. A. Wayne, M. J. Stevens, T. Gerrits, S. Glancy, D. R. Hamel, M. S. Allman, K. J. Coakley, S. D. Dyer, C. Hodge, A. E. Lita, V. B. Verma, C. Lambrocco, E. Tortorici, A. L. Migdall, Y. Zhang, D. R. Kumor, W. H. Farr, F. Marsili, M. D. Shaw, J. A. Stern, C. Abellán, W. Amaya, V. Pruneri, T. Jennewein, M. W. Mitchell, P. G. Kwiat, J. C. Bienfang, R. P. Mirin, E. Knill, and S. W. Nam, *Phys. Rev. Lett.* **115**, 250402 (2015).

[7] W. Rosenfeld, D. Burchardt, R. Garthoff, K. Redeker, N. Ortegel, M. Rau, and H. Weinfurter, *Phys. Rev. Lett.* **119**, 010402 (2017).

[8] M.-H. Li, C. Wu, Y. Zhang, W.-Z. Liu, B. Bai, Y. Liu, W. Zhang, Q. Zhao, H. Li, Z. Wang, L. You, W. J. Munro, J. Yin, J. Zhang, C.-Z. Peng, X. Ma, Q. Zhang, J. Fan, and J.-W. Pan, *Phys. Rev. Lett.* **121**, 080404 (2018).

[9] Ü. Vazirani and T. Vidick, *Phys. Rev. Lett.* **113**, 140501 (2014).

[10] “Homodyne detection,” in *A Guide to Experiments in Quantum Optics* (John Wiley & Sons, Ltd, 2019) Chap. 9, pp. 303–376.

[11] S. L. Braunstein and P. van Loock, *Rev. Mod. Phys.* **77**, 513 (2005), publisher: American Physical Society.

[12] A. Gilchrist, P. Deuar, and M. D. Reid, *Phys. Rev. Lett.* **80**, 3169 (1998).

[13] W. J. Munro, *Phys. Rev. A* **59**, 4197 (1999).

[14] J. Wenger, M. Hafezi, F. Grosshans, R. Tualle-Brouri, and P. Grangier, *Phys. Rev. A* **67**, 012105 (2003).

[15] R. García-Patrón, J. Fiurášek, N. J. Cerf, J. Wenger, R. Tualle-Brouri, and P. Grangier, *Phys. Rev. Lett.* **93**, 130409 (2004).

[16] R. García-Patrón, J. Fiurášek, and N. J. Cerf, *Phys. Rev. A* **71**, 022105 (2005).

[17] E. G. Cavalcanti, C. J. Foster, M. D. Reid, and P. D. Drummond, *Phys. Rev. Lett.* **99**, 210405 (2007).

[18] A. Acín, N. J. Cerf, A. Ferraro, and J. Niset, *Phys. Rev. A* **79**, 012112 (2009).

[19] J. Etesse, R. Blandino, B. Kanseri, and R. Tualle-Brouri, *New Journal of Physics* **16**, 053001 (2014).

[20] E. Oudot, G. Massé, X. Valcarce, and A. Acín, “Realistic bell tests with homodyne measurements,” (2024), arXiv:2402.01530 [quant-ph].

[21] J. F. Clauser, M. A. Horne, A. Shimony, and R. A. Holt, Phys. Rev. Lett. **23**, 880 (1969).

[22] N. D. Mermin, Phys. Rev. Lett. **65**, 1838 (1990).

[23] D. Klyshko, Physics Letters A **218**, 119 (1996).

[24] S. Abramsky, R. S. Barbosa, and S. Mansfield, Phys. Rev. Lett. **119**, 050504 (2017).

[25] R. S. Barbosa, T. Douce, P.-E. Emeriau, E. Kashefi, and S. Mansfield, Commun. Math. Phys. **391**, 1047 (2022).

[26] A. Fine, Phys. Rev. Lett. **48**, 291 (1982).

[27] S. Abramsky and A. Brandenburger, New Journal of Physics **13**, 113036 (2011).

[28] D. Collins, N. Gisin, N. Linden, S. Massar, and S. Popescu, Phys. Rev. Lett. **88**, 040404 (2002).

[29] B. S. Tsirel'son, Journal of Soviet Mathematics **36**, 557 (1987).

[30] A. Cavaillès, H. Le Jeannic, J. Raskop, G. Guccione, D. Markham, E. Diamanti, M. D. Shaw, V. B. Verma, S. W. Nam, and J. Laurat, Phys. Rev. Lett. **121**, 170403 (2018).

[31] M. Moradi, J. Camilo López Carreño, A. Buraczewski, T. McDermott, B. Elisabeth Asenbeck, J. Laurat, and M. Stobińska, New Journal of Physics **26**, 033019 (2024).

[32] N. Brunner, D. Cavalcanti, S. Pironio, V. Scarani, and S. Wehner, Rev. Mod. Phys. **86**, 419 (2014).

[33] S. KOCHEN and E. P. SPECKER, Journal of Mathematics and Mechanics **17**, 59 (1967).

[34] R. W. Spekkens, Phys. Rev. A **71**, 052108 (2005).

[35] S. Popescu and D. Rohrlich, Foundations of Physics **24**, 379 (1994).

[36] A. Ketterer, A. Lavasanne-Finot, and L. Aolita, Phys. Rev. A **97**, 012133 (2018).

[37] C. E. Lopetegui-González, “cLopetegui/CV_contextuality_sdp,” (2025).

[38] Y.-S. Ra, A. Dufour, M. Walschaers, C. Jacquard, T. Michel, C. Fabre, and N. Treps, Nat. Phys. **16**, 144 (2020).

[39] C. Fabre and N. Treps, Rev. Mod. Phys. **92**, 035005 (2020).

[40] A. Aralov, Émilie Gillet, V. Nguyen, A. Cosentino, M. Walschaers, and M. Frigerio, “Photon catalysis for general multimode multi-photon quantum state preparation,” (2025), arXiv:2507.19397 [quant-ph].

[41] D. Gottesman, A. Kitaev, and J. Preskill, Phys. Rev. A **64**, 012310 (2001).

[42] M. V. Larsen, J. E. Bourassa, S. Kocsis, J. F. Tasker, R. S. Chadwick, C. González-Arciniegas, J. Hastrup, C. E. Lopetegui-González, F. M. Miatto, A. Motamedi, R. Noro, G. Roeland, R. Baby, H. Chen, P. Contu, I. Di Luch, C. Drago, M. Giesbrecht, T. Grainge, I. Krasnokutska, M. Menotti, B. Morrison, C. Puviraj, K. Rezaei Shad, B. Hussain, J. McMahon, J. E. Ortmann, M. J. Collins, C. Ma, D. S. Phillips, M. Seymour, Q. Y. Tang, B. Yang, Z. Vernon, R. N. Alexander, and D. H. Mahler, Nature **642**, 587 (2025), publisher: Nature Publishing Group.

[43] C. Flühmann, T. L. Nguyen, M. Marinelli, V. Negnevitsky, K. Mehta, and J. P. Home, Nature **566**, 513 (2019), publisher: Nature Publishing Group.

[44] M. Kudra, M. Kervinen, I. Strandberg, S. Ahmed, M. Scigliuzzo, A. Osman, D. P. Lozano, M. O. Tholén, R. Borgani, D. B. Haviland, G. Ferrini, J. Bylander, A. F. Kockum, F. Quijandría, P. Delsing, and S. Gasparinetti, PRX Quantum **3**, 030301 (2022).

[45] S. Touzard, A. Grimm, Z. Lehtas, S. O. Mundhada, P. Reinhold, C. Axline, M. Reagor, K. Chou, J. Blumoff, K. M. Sliwa, S. Shankar, L. Frunzio, R. J. Schoelkopf, M. Mirrahimi, and M. H. Devoret, Phys. Rev. X **8**, 021005 (2018).

[46] Y. Yang, I. Kladarić, M. Drimmer, U. von Lüpke, D. Lenterman, J. Bus, S. Marti, M. Fadel, and Y. Chu, Science **386**, 783 (2024).

[47] I. Strandberg, A. M. Eriksson, B. Royer, M. Kervinen, and S. Gasparinetti, Phys. Rev. Lett. **133**, 063601 (2024).

[48] D. M. Greenberger, M. A. Horne, A. Shimony, and A. Zeilinger, American Journal of Physics **58**, 1131 (1990).

[49] G. Guccione, T. Darras, H. L. Jeannic, V. B. Verma, S. W. Nam, A. Cavaillès, and J. Laurat, Science Advances **6**, eaba4508 (2020).

[50] T. Darras, B. E. Asenbeck, G. Guccione, A. Cavaillès, H. Le Jeannic, and J. Laurat, Nature Photonics **17**, 165 (2023), publisher: Nature Publishing Group.

[51] G. de Gliniasty, P. Hilaire, P.-E. Emeriau, S. C. Wein, A. Salavrakos, and S. Mansfield, Quantum **8**, 1423 (2024).

[52] G. Müller-Rigat, A. Aloy, M. Lewenstein, and I. Frerot, PRX Quantum **2**, 030329 (2021).

Appendix A: Moment based SDP

The primal program at level k in the hierarchy is given by

$$(SP_k) \left\{ \begin{array}{l} \sup_{\mathbf{y} \in \mathbb{R}^{s(k)}} y_0 \\ \text{s.t. } \forall C \in \mathcal{M}, M_k(y^{e,C} - y|_C) \succeq 0 \\ \quad M_k(y) \succeq 0 \\ \quad \forall j \in \{1, \dots, m\}, M_{k-r_j}(P_j y) \succeq 0, \end{array} \right. \quad (A1)$$

where P_j is the set of algebraic conditions defining the compact set in which the problem is evaluated. In the case in which we solve the problem in $\mathbb{R}^{|X|}$ this set of constraints is no present. The dual program can be written, after some manipulations, as

$$(SD_k) \left\{ \begin{array}{l} \text{Find } (f_c) \subset \Sigma^2 \mathbb{R}[x]_k, (\sigma_j) \subset \Sigma^2 \mathbb{R}[x]_{k-r_j} \\ \inf \sum_C \int_{O_C} f_C d\mu_C \\ \text{s.t. } \sum_C f_C - \mathbf{1} = \sigma_0 + \sum_{j=1}^m \sigma_j P_j. \end{array} \right. \quad (A2)$$

Here σ_j can be dropped if we consider optimization on $\mathbb{R}^{|X|}$. $\Sigma^2 \mathbb{R}[x]_k$ refers to the set of SOS polynomials of order $2k$. From here it is possible to recover again a Bell inequality. If the empirical model is non contextual the

constraint implies that

$$\begin{aligned}
 B(e_C) &= 1 - \sum_C \int_{O_C} f_C d e_C \\
 &= 1 - \int_{O_C} \left(1 + \sigma_0 + \sum_{j=1}^m \sigma_j P_j \right) d e_C \quad (A3) \\
 &= - \int_{O_C} \left(\sigma_0 + \sum_{j=1}^m \sigma_j P_j \right) d e_C \leq 0.
 \end{aligned}$$

More generally the Bell inequality is just given by the first line above, which can be extracted from the program.

1. Results

Our exploration of this tool on continuous variable systems started from using the moment based SDP (A1). Nevertheless, so far we have not managed to observe any non-zero contextual fraction on some quantum behavior. On the other hand, it is interesting to notice that contextual behaviors beyond the set of quantum correlations can be detected using this program.

Popescu-Rohrlich boxes [35], provide a maximally contextual empirical model in discrete variables. Continuous variable generalizations of those probabilistic behaviors can be constructed quite naturally. Below we can see the table

	00	01	10	11
(a_1, b_1)	$1/2$	0	0	$1/2$
(a_1, b_2)	$1/2$	0	0	$1/2$
(a_2, b_1)	$1/2$	0	0	$1/2$
(a_2, b_2)	0	$1/2$	$1/2$	0

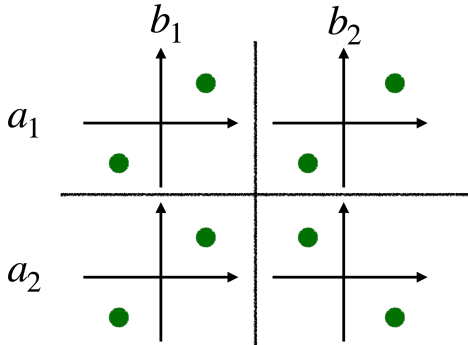


FIG. 12. PR behavior in its discrete and continuous generalization.

The continuous generalization of the PR box can be parametrized as

$$p_{pr}^C(\mathbf{x}_C) = \frac{1}{4\pi\sigma^2} \left(e^{-\frac{|\langle \mathbf{x}_C + (a, (-1^{ij})a) \rangle|^2}{2\sigma^2}} + e^{-\frac{|\langle \mathbf{x}_C - (a, (-1^{ij})a) \rangle|^2}{2\sigma^2}} \right) \quad (A4)$$

where a represents the center of the peaks of the distributions, and σ their variance, which we consider homogeneous along both directions. When evaluating the contextual fraction of such states, for small σ we obtain $CF = 1$, and such a behavior persists up to large variances, as can be observed in Fig.13. The plot corresponds to the case in which we pick $a = 1$. Naturally, as σ increases, the value of the contextual fraction decreases. This happens beyond some point, at which the peaks of the distributions start to overlap. The threshold beyond which contextuality is no longer observed increases with K for small values of K . In Fig.14, we can observe the histograms for values of sigma below and above the threshold. Moreover, we can observe that the threshold decreases with the spacing between the peaks of the distribution, from a similar reason.

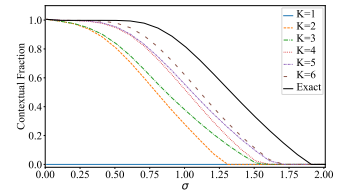


FIG. 13. Each line in the plot represents the value of the contextual fraction of the empirical behavior associated to a PR box, evaluated at different levels K of the hierarchy of SDP's. The plots are evaluated against the variance σ of the peaks of the distribution. All peaks are located at $(\pm 2, \pm 2)$. Even at the first non-trivial order in the hierarchy ($K = 2$), the SDP converges to the exact value, for small σ . For large values of σ , on the other hand, there is a finite gap between the exact value, computed using the *LP* implementation, and the values obtained using $K \leq 6$.

For each run of the program that returns a non-zero contextual fraction, we obtain a polynomial Bell inequality, following the recipe described in section A. These moment based Bell inequalities can be optimized within the set of quantum states with a finite cutoff on Fock space. Nevertheless, all the Bell inequalities obtained are trivial for the set of quantum states up to the cutoff considered $N_{max} = 50$. An other degree of freedom to consider is the homodyne settings with respect to which the inequalities are optimized. Nevertheless, an exhaustive exploration over this degree of freedom provided no positive results.

Other finite behaviors, previously reported to display contextuality as discrete probability measures, were also extended to the continuous case, following a similar procedure as for the PR boxes. None of the Bell inequalities obtained provided any non-zero contextual fraction for a quantum state. Other extensions were considered by mixing the continuous versions of discrete non-local behaviors with continuous variable behaviors expected to be non-local. In this way, one would expect to obtain non-trivial Bell inequalities, yet the results proved negative as well.

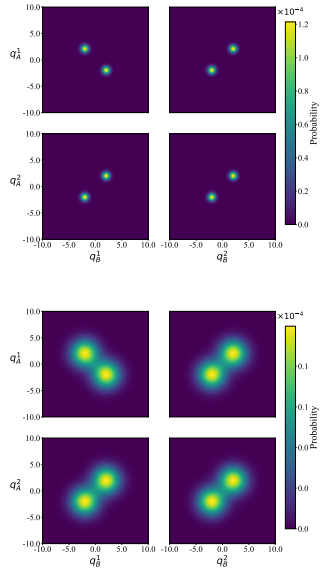


FIG. 14. Continuous extensions of the PR empirical models, for two different peak widths, *i.e.*, different values of σ in equation (A4). The values correspond to the probability for each bin, provided the accuracy with which the plot is constructed ($\delta q = 1.95 \times 10^{-2}$). The left plots correspond to $\sigma = 0.5$, for which maximum contextuality is obtained. The right plots correspond to $\sigma = 1.75$, slightly above the limit beyond which no contextuality is observed. Notice that this starts happening when the overlap between the peaks is different from zero. Nevertheless, the exact value of the contextual fraction is a high one.

Appendix B: Optimal qutrit state for CGLMP Bell inequality using Pauli measurements

In [28], the authors propose explicit expressions for states and qudit measurement results. They show that these states violate some Bell inequalities that they propose. The measurements that they propose to perform

are not Pauli measurements, which would be desired when trying to find a mapping to a CV encoding. Also, the Bell inequality is not in operator form, but rather constructed in a way similar to the one we use in this paper, by making the filters that parametrize the Bell inequality explicit for each outcome. We divide the procedure to find an optimal CV realization in the following steps:

1. Find an explicit operator expression for the CGLMP Bell inequality for the optimal states and measurements.
2. Use the same expression for constructing the Bell operator but using generalized Pauli operators X, Z , instead of the optimal measurements, and construct the “Pauli” Bell operator. For this operators find the maximum eigenvalue and its corresponding eigenvector, which parametrizes the optimal state for this Bell inequality.
3. Construct a CV encoded version of this state using a qutrit GKP state.

The procedure described above is implemented in one of the examples in the GitHub repository [37]. The explicit expression for the qudit state is

$$\begin{aligned}
 |\psi\rangle = & (-0.22081098 + 0.382455814i)|0,0\rangle \\
 & + (0.01050768 - 0.164565746i)|0,1\rangle \\
 & + (0.31141613 + 0.118874310i)|0,2\rangle \\
 & + (0.31141611 + 0.118874303i)|1,0\rangle \\
 & + 0.44162192)|1,1\rangle \\
 & + (0.13726426 + 0.0913827838i)|1,2\rangle \\
 & + (0.01050767 - 0.164565737i)|2,0\rangle \\
 & + (-0.25865624 + 0.210257131i)|2,1\rangle \\
 & + (0.44162195)|2,2\rangle.
 \end{aligned}$$